Dalton Transactions

PAPER

View Article Online
View Journal | View Issue



Cite this: *Dalton Trans.*, 2014, **43**, 10930

# Manganese-mefenamic acid complexes exhibit high lipoxygenase inhibitory activity†

Jie Feng, Xin Du, Hui Liu, Xin Sui, Chen Zhang, Yun Tang and Jingyan Zhang*

The coordination of non-steroidal anti-inflammatory drugs (NSAIDs) to metal ions could improve the pharmaceutical efficacy of NSAIDs due to the unique characteristics of metal complexes. However, the structures of many metal-NSAID complexes are not well characterized; the functional mechanism and pharmaceutical effect of these complexes thus are not fully understood. In this work, three manganese-mefenamic acid (Mn-mef) complexes were synthesized and structurally characterized, and their pharmaceutical effect was investigated. We found that the three Mn-mef complexes exhibit higher lipoxygenase (LOX-1) inhibitory activity ($IC_{50}$ values are 16.79, 38.63 and 28.06 μM, respectively) than the parent ligand mefenamic acid (78.67 μM). More importantly, the high inhibitory activity of the Mn-mef complexes is closely related to their spatial arrangements, which determine their interaction with LOX-1. Computer docking of the Mn-mef complexes with the LOX-1 confirms the experimental results: smaller Mn-mef complexes tend to bind competitively to LOX-1 at the substrate binding site, which is also analogous to the binding of the ligand mefenamic acid, while the bulky metal complexes inhibit the enzyme activity un-competitively. In addition, the Mn-mef complexes exhibit higher anti-oxidant activity than the ligand mefenamic acid. The higher anti-oxidant activity of the Mn-mef complexes apparently originated from the manganese centre of the complexes. We thus conclude that Mn-mef complexes enhance the anti-inflammatory activity of mefenamic acid by increasing their activity *via* changing their interaction mode with the enzymes, and/or by improving their anti-oxidant ability using metal ions. This work provides experimental evidence that with the unique spatial arrangements, metal-NSAID complexes could interact with the target enzymes more specifically and efficiently, which is superior to their parent NSAID ligand.

Received 15th April 2014,
Accepted 16th May 2014

DOI: 10.1039/c4dt01111b

www.rsc.org/dalton

## Introduction

Non-steroidal anti-inflammatory drugs (NSAIDs) that are employed to alleviate inflammation and pain associated with diseases exert their therapeutic effects by inhibiting prostaglandin and thromboxane synthesis, which were derived from the enzymatic transformation of arachidonic acid by cyclooxygenase (COX) and lipoxygenase (LOX) enzymes, respectively.[1–4] However, NSAID-induced side effects, particularly in the gastrointestinal tract and the kidney, often limit their applications.[5,6] For that reason, considerable efforts have been made to increase their potency while minimizing their side effects. Chemical modification of the structure of NSAIDs is an often used strategy to improve the performance of NSAIDs,[7,8] while the coordination of NSAIDs to metal ions is one of the fast developing methods because the divalent metal ions may impose extra properties to the NSAID ligands.[9] In comparison with NSAIDs, metal-NSAID complexes have many more coordination numbers, geometries, and oxidation/reduction states that can be used to create structures that interact with targets in unique ways. These are unavailable to most NSAIDs. Numerous metal complexes with NSAIDs as ligands have shown to be more potent than either the parent NSAID ligands or the un-complexed metal salts. For example, Regtop *et al.* found that copper and zinc complexes of indomethacin could improve the pharmacological profiles of indomethacin and reduce its toxicity.[10] Konstandinidou *et al.* reported that the anti-inflammatory activity of diclofenac could be enhanced by the coordination with $Co^{2+}$, $Ni^{2+}$, and $Pd^{2+}$ ions, because these metal complexes could offer significant protection against lipid peroxidation *in vitro*.[11] Some Cu-NSAID complexes also exhibit potent SOD or anti-inflammatory activity.[9,12] However, the structures of the metal-NSAID com-

*State Key Laboratory of Bioreactor Engineering, Shanghai Key Laboratory of New Drug Design, School of Pharmacy, East China University of Science and Technology, Shanghai, 200237, P. R. China. E-mail: jyzhang@ecust.edu.cn; Fax: +86-021-64253846*

†Electronic supplementary information (ESI) available: The line weaver-Burk plot for the inhibition of LOX-1 by complexes **1–3**; the docking area in this work, and the spatial environment of the complex **1** docked inside the cavity $II_a$ of LOX-1; DPPH radical scavenging by the complexes **1–3**; the SOD inhibitory activity, and the selected IR data for the complexes **1–3**. CCDC 931669, 931670 and 955463. For ESI and crystallographic data in CIF or other electronic format see DOI: 10.1039/c4dt01111b

plexes in most cases are not well characterized, some of them are just the mixtures of the metal salts and NSAIDs; hence the improvement of the anti-inflammatory activity of NSAIDs by the coordination to metal ions is not well understood.

Mefenamic acid (2-(2,3-dimethylphenyl)aminobenzoic acid, mef) is one of the most effective NSAIDs that are used in clinics, and exhibits favourable anti-inflammatory and analgesic properties, but it also exhibits side effects as other NSAIDs.[13] Kovala-Demertzi *et al.* made attempts to improve its activity and decrease its side effects by preparing its different complexes with metal ions including $Cu^{2+}$, $Zn^{2+}$, $Mn^{2+}$, $Co^{2+}$, and $Ni^{2+}$. Their biological responses in terms of antioxidant activity, LOX inhibition, and trypsin induced proteolysis were compared; the anti-proliferative activity and anti-inflammatory activity of some compounds were also investigated.[14] Later, Psomas *et al.* from the same university also reported Co-mef and Cu-mef complexes.[15,16] In that work, they focused more on the interaction of these complexes with DNA and bovine serum albumin in addition to their anti-oxidant and LOX inhibitory activities. Spectroscopic analysis and the pharmacological activity of the Sn-mef complex were also reported,[17] but tin itself is a toxic element exerting profound adverse effects on many life processes.[18] Though excess manganese in the brain may also induce permanent neurodegenerative damage, resulting in a syndrome similar to Parkinson's disease,[19] manganese is an essential trace element for human beings and a cofactor for a number of enzymes.[20] Many metal-mef complexes have been reported so far; most of them are not structurally defined, and their biological response and pharmaceutical properties could not be correlated well with their structures, or tuned according to their structures.

In this study, three Mn-mef complexes, $Mn(mef)_2(CH_3OH)_4$ (**1**), $Mn(mef)_2(bipy)(CH_3OH)_2$ (**2**), and $Mn(mef)_2(phen)H_2O$ (**3**) (bipy = 2,2′-bipyridyl, phen = phenanthroline), were structurally well characterized, and their LOX-1 inhibitory activity and antioxidant ability were examined experimentally in parallel with the parent drug mefenamic acid. The binding of the three complexes to the LOX-1 was investigated *via in silico* docking as well. The results clearly indicated that Mn-mef complexes exhibit high LOX-1 inhibitory activity than mefenamic acid, which can be attributed to the different interaction modes of the Mn-mef complexes with LOX-1. Manganese is a less toxic element;[21] Mn-mef complexes hence show great promise as pharmaceutical reagents.

# Experimental section

### Materials and methods

All reagents and organic solvents were of analytical grade and used as received without further purification. 1,1-Diphenyl-2-picrylhydrazyl (DPPH) was purchased from Alfa Aesar Company, lipoxygenase (EC 1.13.11.12, LOX-1) was obtained from Sigma-Aldrich Company, and the others were from Sino-Pharm Chemical Reagent Co., Ltd. Superoxide dismutase (SOD) assay kit was purchased from Jiancheng Bioengineering Institute (Nanjing, China). Electronic absorption spectra were recorded on a Cary 50 spectrophotometer with quartz cuvettes (Varian, USA). Elemental analyses of the all complexes were performed with an elementar vario EL III analyzer (Germany). X-band EPR spectra were acquired on an EMS spectrometer (Bruker, USA) with a cryostat ESR-900 system (Oxford, UK). Conductivity measurements were carried out with a HI8733 conductivity meter using methanol as a solvent. X-ray crystallographic data of the complexes were collected on a SMART diffractometer (Bruker, USA) using Mo-Kα radiation ($\lambda$ = 0.71 Å). The structure was solved by direct methods (SHELXS-97) and refined with full-matrix least-squares techniques on $F^2$ using SHELXL-97. Mass spectrometry data were acquired using a LCQ Deca XP Plus Quadrupole Ion Trap Mass Spectrometer (Thermo Finnigan, USA).

### Preparation of Mn-mef complexes

**$Mn(mef)_2(CH_3OH)_4$ (1).** Mefenamic acid (0.4 mmol, 96.4 mg) and KOH (0.4 mmol, 22.4 mg) were added to 15 mL of methanolic solution and stirred for 1 h. The solution was then added to a methanolic solution (10 mL) of $MnCl_2{\cdot}4H_2O$ (0.2 mmol, 39.5 mg). The reaction mixture was stirred for 2 h at room temperature. The resulting solution was filtered; light-yellow block crystals suitable for X-ray structure analysis were obtained by slow evaporation of the filtrate, collected by filtration, washed with diethyl ether and dried in air. Yield: 53.75% (based on the manganese salts). Elemental analysis data: calculated (%) for $C_{34}H_{44}MnN_2O_8$ ($M_w$ 663.25): C, 61.53; H, 6.68; N, 4.22. Found (%): C, 61.28; H, 6.54; N, 4.22.

**$Mn(mef)_2(bipy)(CH_3OH)_2$ (2).** A methanolic solution (15 mL) of mefenamic acid (0.4 mmol, 96.4 mg) and KOH (0.4 mmol, 22.4 mg) was stirred for 1 h. This solution was then mixed with a methanolic solution of 2,2′-bipyridyl (0.2 mmol, 31.2 mg) and a methanolic solution (10 mL) of $MnCl_2{\cdot}4H_2O$ (0.2 mmol, 39.5 mg). The obtained solution was stirred for 2 h and filtered. Light-yellow well-shaped crystals that were suitable for X-ray diffraction were obtained after three weeks. The crystals were collected by filtration, washed with diethyl ether and dried in air. Yield: 67.55% (based on the manganese salts). Elemental analysis data: calculated (%) for $C_{42}H_{44}MnN_4O_6$ ($M_w$ 755.75): C, 66.75; H, 5.87; N, 7.41. Found (%): C, 66.43; H, 5.53; N, 7.54.

**$Mn(mef)_2(phen)H_2O$ (3).** The complex **3** was obtained with the same procedure used for the complex **2** but using phenanthroline (0.2 mmol, 39.6 mg) instead of 2,2′-bipyridyl. The reaction mixture was filtered and washed with water. Then the filtration was dissolved in DMF for slow evaporation. The microcrystalline product was collected after a few days, washed with a small amount of methanol and dried in air, making it just suitable for X-ray diffraction. Yield: *ca.* 48%. Elemental analysis data: calculated (%) for $C_{42}H_{38}MnN_4O_5$ ($M_w$ 733.70): C, 68.75; H, 5.22; N, 7.64. Found (%): C, 69.07; H, 5.39; N, 7.49.

The corresponding three Co-mef complexes were synthesized and characterized according to the literature.[15]

### Mass spectrometry

All mass spectra were collected on a Quadrupole Ion Trap Mass Spectrometer (Thermo Finnigan, USA) fitted with an electrospray interface and operated in the positive ionization mode. Samples were all dissolved in DMF and applied *via* a direct infusion method at a flow rate of 3 μL $min^{-1}$. The analysis was performed using the following parameters: spray voltage, 4.8 kV; capillary temperature, 275 °C; capillary voltage, 15 V. And nitrogen was used as the nebulizer gas.

### LOX-1 inhibition

LOX-1 ($10^{-6}$ mM) was added to borate buffer (0.1 M, pH 9.0) containing different concentrations of the complexes (complexes **1**, **2** or **3**). The reaction was initiated by adding the substrate linoleic acid (0.75 mM), and the absorbance at 235 nm was measured after 5 min of the reaction in the dark. The inhibition of the complexes was determined by the equation: lipoxygenase activity (%) = $(A'/A_0) \times 100$, where $A'$ is the absorbance of the reaction with the complex and $A_0$ is the absorbance of the reaction without the complex, respectively.[22]

### Computer docking

The docking experiments were performed using the free trial of Molegro Virtual Docker software (MVD; version-6.0) obtained from the homepage of Molegro (http://www.clcbio.com/products/molegro-virtual-docker/#trial). The crystal structure of LOX-1 was downloaded from the PDB protein data bank (PDB ID: 1F8N). The crystal structures of the complex were converted as the MOL format using the Diamond software. The water molecules in LOX-1 were removed and explicit hydrogen atoms were added to the complexes during the preparation by MVD. The docking of the complexes with LOX-1 was performed in the vicinity of the active site of LOX-1 based on the previously published crystal structure of LOX-1.[23] A sphere with a radius of 25 Å that was centered at the Fe atom (coordination in the LOX-1: 24.53, 44.38, 10.60) of the LOX-1, covering the whole active site of LOX-1 and almost the whole C-domain, was employed as the docking area in the LOX-1. Docking calculations were carried out using the heuristic search algorithm MolDock SE (simplex evolution), which was used as a search algorithm in combination with the grid-based version of the MolDock Scores [GRID] in the analysis.[24] Once the complex and LOX-1 were imported to the program, structural parameters including bond type, hybridization, explicit hydrogen atoms, charges, and flexible torsions were assigned using the automatic preparation function in the MVD software. The grid resolution was set to 0.30 Å; the maximum population size and interactions were set to 50 and 1500, respectively. In the ligand map, the hydrogen bonding and steric minimum strength were set to 0.625. Ten independent runs were carried out for each docking. During the docking, the complexes were treated as flexible molecules, whereas the LOX-1 was regarded rigid.[24] The best docking results were selected on the basis of the MolDock Score, Rerank Score and hydrogen bond.[25]

### Anti-oxidant activity

The solutions were prepared as the following: 0.5 mL methanolic solution of the complex (0.2 mM) was mixed with DPPH methanolic solution (60 μM, 0.5 mL) in the dark. The samples were incubated at 25 °C for 30 min in the dark to reach the equilibrium before the measurement. The radical scavenging ability ($I$) of the three complexes was calculated using the equation: $I\% = (1 - A_s/A_0) \times 100$, where $A_0$ is the absorbance of the sample at 0 min and $A_S$ is the absorbance of the sample at 30 min, respectively.

A commercial superoxidase (SOD) kit was used to measure the $O_2^-$ scavenging ability of the complexes **1–3** and mefenamic acid. $O_2^-$ was generated by xanthine–xanthine oxidase through oxidizing hydroxylamine to nitrite, which has a sharp absorbance at 550 nm after the reaction with the color-developing agent. The percentage of SOD inhibitory activity is calculated according to the equation: SOD inhibitory activity (%) = $(A_{blank} - A_{sample})/A_{blank} \times 100$.

## Results and discussion

### Structures of the Mn-mef complexes

The structures of the complexes **1–3** were determined by single crystal X-ray diffraction (detailed crystallographic data and the structures are given in Table 1 and Fig. 1, respectively). Selected bond lengths and angles of the complexes are summarized in Table 2. As shown in Fig. 1, the complex **1** is a centrosymmetric mononuclear manganese complex with two mef ligands and four methanol molecules. There are two methanol molecules in the unit cell of the crystal of the complex **1**. The manganese centre is in a six coordinated octahedral geometry. The four equatorial sites are occupied by two oxygen atoms of

Table 1 Crystallographic data for the complexes **1–3**

| Parameter | **1** | **2** | **3** |
|---|---|---|---|
| Empirical formula | $C_{36}H_{52}MnN_2O_{10}$ | $C_{42}H_{44}MnN_4O_6$ | $C_{42}H_{38}MnN_4O_5$ |
| Formula weight | 727.74 | 755.75 | 733.70 |
| Crystal system | Triclinic | Orthorhombic | Triclinic |
| Space group | $P\bar{1}$ | $Iba2$ | $P\bar{1}$ |
| $a$ (Å) | 7.733(15) | 7.425(4) | 9.584(4) |
| $b$ (Å) | 8.013(16) | 29.560(2) | 12.224(5) |
| $c$ (Å) | 15.932(3) | 17.582(14) | 15.873(7) |
| $\alpha$ (°) | 91.59(3) | 90 | 96.746(7) |
| $\beta$ (°) | 95.39(3) | 90 | 96.434(8) |
| $\gamma$ (°) | 92.27(3) | 90 | 97.868(8) |
| Volume (Å$^3$) | 981.5(3) | 3859.1(5) | 1806.8(13) |
| $Z$ | 1 | 4 | 2 |
| Reflections collected | 7049/4310 [$R$(int) = 0.0569] | 8896/4167 [$R$(int) = 0.0466] | 9150/6323 [$R$(int) = 0.0455] |
| Data/restraints/parameters | 4310/0/228 | 4167/8/243 | 6323/0/479 |
| GOF on $F^2$ | 0.965 | 0.875 | 1.024 |
| Final $R$ indices [$I > 2\sigma(I)$] | $R_1$ = 0.0703, w$R_2$ = 0.1639 | $R_1$ = 0.0493, w$R_2$ = 0.913 | $R_1$ = 0.0534, w$R_2$ = 0.691 |
| $R$ indices (all data) | $R_1$ = 0.1243, w$R_2$ = 0.1868 | $R_1$ = 0.1188, w$R_2$ = 0.1045 | $R_1$ = 0.1360, w$R_2$ = 0.789 |
| CCDC no. | 931669 | 931670 | 955463 |

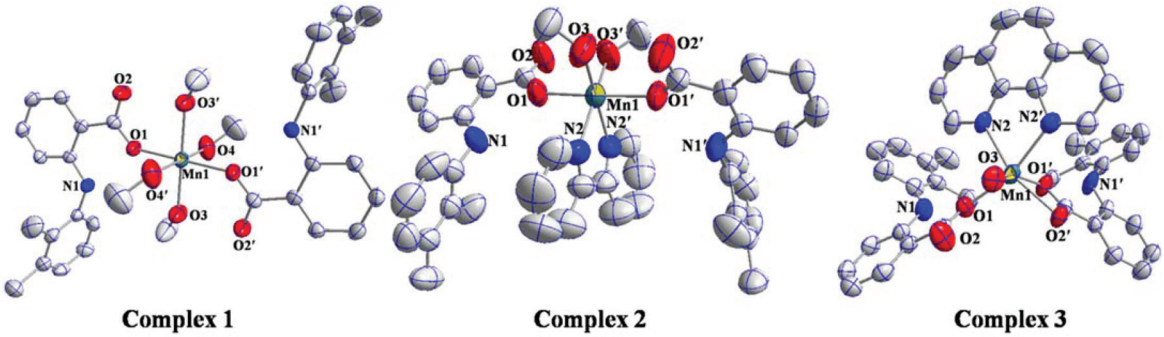


Fig. 1 Crystal structures of the complexes **1–3**.

Table 2 Selected bond distances (Å) and angles (°) for compounds **1–3**

| **1** | | **2** | | **3** | |
|---|---|---|---|---|---|
| Mn(1)–O(1) | 2.129(19) | Mn(1)–O(1) | 2.126(2) | Mn(1)–O(1) | 2.100(2) |
| Mn(1)–O(1′) | 2.129 (19) | Mn(1)–O(1′) | 2.126(2) | Mn(1)–O(1′) | 2.267(2) |
| Mn(1)–O(3) | 2.202(2) | Mn(1)–O(3) | 2.141(4) | Mn(1)–O(2′) | 2.220 (2) |
| Mn(1)–O(4) | 2.213(3) | Mn(1)–O(3′) | 2.141(4) | Mn(1)–O(3) | 2.159(3) |
| Mn(1)–O(4′) | 2.213(3) | Mn(1)–N(2) | 2.232(4) | Mn(1)–N(2) | 2.270(3) |
| Mn(1)–O(3′) | 2.202(2) | Mn(1)–N(2′) | 2.232(4) | Mn(1)–N(2′) | 2.262(3) |
| O(1)–Mn(1)–O(1′) | 180.00 | O(1)–Mn(1)–O(1′) | 177.4(2) | O(1)–Mn(1)–O(1′) | 96.79(9) |
| O(1)–Mn(1)–O(3) | 92.35(8) | O(1′)–Mn(1)–O(3′) | 92.13(13) | O(1)–Mn(1)–O(2′) | 103.00(8) |
| O(1)–Mn(1)–O(3′) | 87.65(8) | O(1)–Mn(1)–O(3′) | 86.14(12) | O(1)–Mn(1)–O(3) | 89.15(10) |
| O(1)–Mn(1)–O(4) | 88.69(9) | O(1′)–Mn(1)–O(3) | 86.15(12) | O(1)–Mn(1)–N(2) | 90.94(10) |
| O(1)–Mn(1)–O(4′) | 91.31(9) | O(1)–Mn(1)–O(3) | 92.12(13) | O(1)–Mn(1)–N(2′) | 162.97(9) |
| O(1′)–Mn(1)–O(3) | 87.65(8) | O(3′)–Mn(1)–O(3) | 96.8(3) | O(3)–Mn(1)–N(2) | 104.97(10) |
| O(1′)–Mn(1)–O(3′) | 92.35(8) | O(1′)–Mn(1)–N(3′) | 88.18(13) | O(3)–Mn(1)–N(2′) | 89.11(11) |
| O(1′)–Mn(1)–O(4) | 91.31(9) | O(1)–Mn(1)–N(3′) | 93.92(14) | N(2)–Mn(1)–N(2′) | 73.17(10) |
| O(1′)–Mn(1)–O(4′) | 88.69(9) | O(3′)–Mn(1)–N(2′) | 95.72(17) | O(1′)–Mn(1)–O(2′) | 58.22(8) |
| O(3)–Mn(1)–O(4) | 89.42(10) | O(3)–Mn(1)–N(2′) | 166.45(17) | O(1′)–Mn(1)–O(3) | 156.79(9) |
| O(3)–Mn(1)–O(4′) | 90.58(10) | O(1′)–Mn(1)–N(2) | 93.91(14) | O(1′)–Mn(1)–N(2) | 97.37(9) |
| O(3′)–Mn(1)–O(4) | 90.58(10) | O(1)–Mn(1)–N(2) | 88.19(13) | O(1′)–Mn(1)–N(2′) | 91.42(10) |
| O(3′)–Mn(1)–O(4′) | 89.42(10) | O(3′)–Mn(1)–N(2) | 166.44(17) | O(2′)–Mn(1)–O(3) | 98.59(9) |
| O(3)–Mn(1)–O(3′) | 180.00 | O(3)–Mn(1)–N(2) | 95.72(17) | O(2′)–Mn(1)–N(2) | 152.77(9) |
| O(4)–Mn(1)–O(4′) | 180.00 | N(2′)–Mn(1)–N(2) | 72.4(2) | O(2′)–Mn(1)–N(2′) | 94.01(9) |

methanol (Mn1–O4(4′), 2.213(3) Å) and two oxygen atoms from the two monodentate mef ligands (Mn1–O1(1′), 2.129(19) Å). The apical positions are occupied by two oxygen atoms of methanol with the Mn1–O3(3′) bond length of 2.202(2) Å. Apparently, the Mn–O bonds formed with mef are stronger than that with methanol molecules. The Mn atom lies below the basal plane by 0.0221 Å. The complex **1** is structurally similar to $Co(mef)_2(MeOH)_4$, except for slightly longer Mn–O distance than Co–O (Co–$O_{carboxylic}$ 2.062(2) Å, Co–$O_{metholic}$ 2.084(3), 2.063(3) Å).[15]

Compared to the complex **1**, the manganese centre in the complex **2** is in a distorted octahedral geometry with a $N_2O_4$ ligand set composed of two O atoms from two mef ligands, two O atoms of methanol, and two N atoms from 2,2′-bipyridyl, which is very similar to cobalt complexes with the same ligands.[15] There are no methanol in the copper complex $[Cu(mef)_2(bipy)]$, instead, the copper atom is six-coordinate and is surrounded by two mef ligands and a bidentate 2,2′-bipyridyl ligand showing a distorted octahedral geometry.[15] In the complex **2**, O3, O3′, N2, and N2′ define a basal plane centred with Mn atom. The Mn–$N_{bipy}$ bond distance (2.232(4) Å) is in good agreement with the same bond reported in the literature,[26] but is longer than Co–$N_{bipy}$ (2.115(3) Å) and Cu–$N_{bipy}$ (1.997(2), 2.006(2) Å).[15,16]The Mn–$O_{metholic}$ bond distance is 2.141(4) Å, which is slightly shorter than that in the complex **1**, while the Mn–$O_{carboxylic}$ bond distance of 2.126(2) Å is comparable to that in the complex **1**. Similar to the complex **1**, the manganese complex **2** has a longer Mn–O bond than cobalt complexes and copper complexes.[15,16] The methanol molecules are lying at *cis* positions (O(3)–Mn(1)–O(3′) = 96.8(3)°) and the oxygen atoms from mefenamic acid are in the *trans* position (O(1)–Mn(1)–O(1′) = 177.4(2)), which is more distorted than that in $Co(mef)_2(bipy)(MeOH)_2$.[15]

The complex **2** is not symmetric, although two oxygen atoms from methanol, two nitrogen and two oxygen atoms from the ligand mef are coordinated equally to the manganese atom. The two mef ligands are orientated in the same direction on the two sides of the Mn-bipy plane, while in the complex **1**, two mef ligands are central symmetric around the manganese centre. The overall structural difference between the complexes **1** and **2** may be caused by the large and flat 2,2′-bipyridyl ligand.

The coordination sphere of the complex **3** is similar to that of the complex **2**, but the manganese ion of the complex **3** has a more distorted octahedral environment with the $N_2O_4$ donor set consisting of two nitrogen atoms from phenanthroline, three oxygen atoms from mefenamic acid and one oxygen atom from methanol. The two mefenamic acid ligands are different, one is a monodentate, while the other one is a bidentate that may lead to the more distorted coordination environment of the manganese centre in the complex **3** compared to the complexes **1**–**2**. The different coordination modes of two mef ligands in the complex **3** also result in the different Mn–O bond distances. The oxygen atom of monodentate mef (Mn(1)–O(1), 2.100(2) Å) is closer to the manganese centre than the oxygen atoms of bidentate mef (Mn(1)–O(1′), 2.267(2); Mn(1)–O(2′), 2.220(2)). As shown in Table 2, the bond angle of N(2)–Mn–N(2′) is in good agreement with the similar structure reported before.[27] Because of the large phenanthroline ligand, the overall structure of the complex **3** is as bulky as the complex **2**, both are much larger than the complex **1**.

### Spectroscopic characterizations

The FT-IR spectra of all the three complexes show two typical broad bands in the ranges of 1609–1613 $cm^{-1}$ and 1385–1391 $cm^{-1}$ due to asymmetric and symmetric C═O vibrations of the mef ligand, respectively. The IR vibrations are summarized in Table S1.† The peak at 3300 $cm^{-1}$ was assigned to N–H vibration, and the peak at 3440 $cm^{-1}$ was assigned to O–H vibration. The stretching modes of three complexes are almost identical, indicating that the coordination of the ligand to the manganese centre is in a similar mode, which is consistent with the elemental analysis and crystal structures. Although in the complex **3**, one of the mef is a bidentate ligand, IR spectra cannot resolve that.

The UV-visible spectra of the complexes **1**–**3** in borate buffer were also recorded as shown in Fig. 2. The bands at 287 and 340 nm in all three complexes were ascribed to the π–π* transition of the mef ligand. In the complex **3**, the band at 265 nm is contributed by the ligand phen. All three complexes do not show absorbance in the visible region (400–800 nm), which is the case for many Mn(II) complexes.[27]

The state of the three complexes in solution was also investigated by electrospray ionization mass spectrometry (ESI-MS), because it is critical for their LOX-1 inhibitory activity. A peak at *m*/*z* 568.2 ($[Mn(mef)_2(CH_3OH)H]^+$) corresponding to the loss of three methanol molecules in the complex **1** was observed. Similarly, the monocations $[Mn(mef)_2(bipy)H]^+$ (*m*/*z* 692.9) and $[Mn(mef)(phen)(DMF)]^+$ (*m*/*z* 548.1) were observed in complexes **2** and **3**, respectively. The results indicate that the ligand mef is coordinated to manganese ions even in solution, however, it is possible that they are in hydrolyzed forms, which cannot be determined from the current data.

### Lipoxygenase inhibitory activity

The functional mechanism of mef is generally believed through inhibition of LOX and/or COX.[28,29] The LOX-1 inhibitory activity of the three complexes was thus examined with linoleic acid as the substrate. The *cis*,*cis*-1,4-pentadiene of linoleic acid can be easily oxidized by LOX-1 to form the *cis*,*trans*-hydroperoxydiene derivative, which shows maximum absorption at 235 nm, and thus can be used as a spectral handle to monitor the LOX-1 activity.[29] The contribution from the complexes at 235 nm was removed by subtracting the spectra of the complexes alone under the same conditions. As shown in Fig. 3, $MnCl_2$ shows no LOX-1 inhibitory activity, while mef and the three Mn-mef complexes show obvious inhibitory activity. $IC_{50}$ values of the mef and the complexes **1**–**3** are 78.67, 16.79, 38.63, and 28.06 μM, respectively. Among them, the complex **1** showed much higher inhibitory activity than the others. For instance, more than 80% activity of LOX-1 was inhibited by 100 μM of the complex **1**, and over 60% and 70% activity of LOX-1 was inhibited under the same concentration of the complexes **2** and **3**, respectively. While for the ligand mef, only about 50% of the activity of LOX-1 was inhibited, suggesting that the Mn-mef complexes are more effective LOX-1 inhibitors than the parent ligand mef. The higher

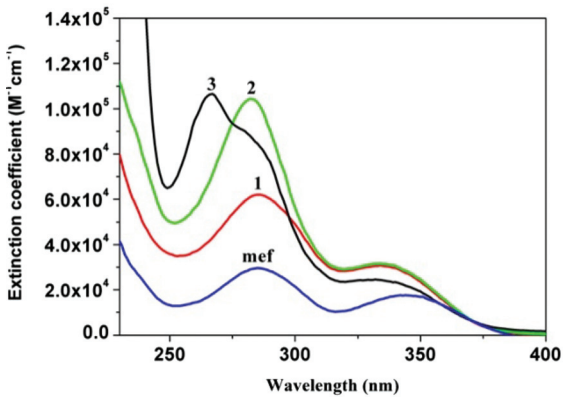


Fig. 2 UV-visible spectra of the complexes **1**–**3** and the ligand mefenamic acid in $H_3BO_3$–NaOH buffer (0.1 M, pH 9.0). The complexes were first dissolved in methanol (complexes **1** and **2**) or DMF (complex **3**), and then 10 μL of the concentrated solution was taken and dispersed into 1 mL of the buffer.

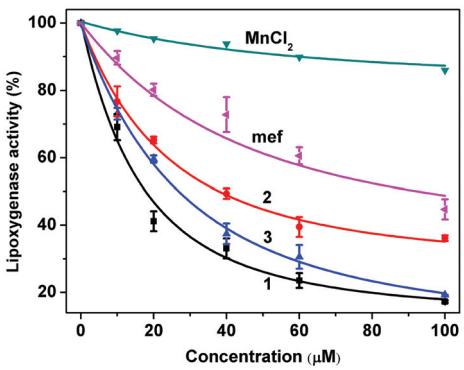


Fig. 3 Comparison of the LOX-1 inhibitory activities of the complexes **1**–**3**, $MnCl_2$, and mefenamic acid. Reaction conditions: linoleic acid (0.75 mM) and LOX-1 ($1 \times 10^{-6}$ mM) in $H_3BO_3$–NaOH buffer (0.1 M, pH 9.0) at 20 °C.

inhibitory activity of the Mn-mef complex could be caused by high concentration of mef, because each Mn-mef complex contains two mef ligands. To exclude this possibility, the state of the Mn-mef complexes in solution was measured by MS spectrometry. It is found that the mef ligand is in the coordinated state in solution.

To understand the inhibition mechanism of the Mn-mef complexes, the kinetics of the LOX-1 was investigated in the absence or presence of the Mn-mef complexes. It is found that $K_m$ of the LOX-1 increased, while $V_{max}$ remains the same in the presence of the complex **1** and mef, while $K_m$ remains the same as that of the native enzyme in the presence of complexes **2** and **3** based on the Line weaver–Bulk plots (Fig. S1†). The values of $K_m$, $V_{max}$, $K_{cat}$ and $K_i$ in the presence of three Mn-mef complexes are summarized in Table 3. Similar kinetics data were obtained when (*Z*)-9-palmitoleyl sulfate inhibited LOX-1.[30] These results indicate that the complex **1** and mef are competitive inhibitors, while complexes **2** and **3** are non-competitive inhibitors. $K_i$ values of the complexes **1–3** and mef also revealed that the order of inhibitory activity is **1** ≫ **2**, **3**, and mef. The highest inhibitory activity and competitive inhibitory mode of the complex **1** suggest that it may interact with LOX-1 in a unique mode.

## Computer docking

To identify the binding mode of the three Mn-mef complexes to LOX-1, computer docking was carried out. The binding site of the natural substrate fatty acid to LOX-1 has long been the subject of debate.[31–33] On the basis of the crystal structure of LOX-1, Boyington *et al.* suggested a narrow passage with sharp bends near the Fe atom and the constriction formed by the side chains is one of the possible binding cavities for the fatty acid substrate (named cavity II, as shown in Fig. S2†).[34] Similarly, the portion of cavity II that is close to the Fe (named cavity $II_a$) was believed as a probable binding site.[35] However, cavity II is wholly internal, and the substrate has to first enter sub-cavity $II_b$ after a rearrangement of the side chains, then pass a convoluted path as much as 40 Å in length to reach cavity $II_a$. The long path and high energy necessary to replace all water molecules in the path made this proposal non-realistic.[35] One promising alternative substrate binding site is at the opposite end of cavity $II_a$, far away from cavity $II_b$ and relatively close to the Fe atom (shown in Fig. S2b†) based on a higher resolution of the crystal structure of LOX.[23] In this case, the access to cavity $II_a$ is only barred 8–10 Å from the Fe atom by a gate composed of three residues from two chains (Thr259, Lys260 and Leu541). This substrate binding site is believed more likely, because the adjustment of the gate is not only sterically unhindered, but also is sufficient to open a wide channel for entry of a fatty acid.[23] We, therefore, docked the substrate linoleic acid, mef and the complexes **1–3** with LOX-1 at the area centering at the atom Fe and covering cavities $II_a$ and $II_b$ (radius of ~25 Å, volume ~$6.5 \times 10^4$ Å$^3$, Fig. S2a†) using the Molegro Virtual Docker program (MVD). The chemical structures of the linoleic acid, mef, and the complexes **1–3** are shown in Fig. 4. The best results showed that linoleic acid could be docked inside cavity $II_a$, and is close to the Fe centre with a distance of 4.27 Å from its pentadiene moiety (C9–13) to Fe atom as shown in Fig. 5a (yellow molecule). The orientation of the linoleic acid is in agreement with the result reported by Minor *et al.*, it bends inside cavity $II_a$ with its tail in the vicinity of the gate (Thr259, Leu260 and Lys541) and the polar head is in the pocket.[23]

The complex **1** was docked in cavity $II_a$ (Fig. 5c, red molecule) similar to the substrate linoleic acid. One mef ligand in the complex **1** takes the same orientation as the linoleic acid. It interacted with Ile751 and Gln495 residues of LOX-1 through hydrogen bonding as shown in Fig. 6a (indicated by blue lines). It also interacted with other residues at the cavity $II_a$ of LOX-1 *via* weak interactions, such as Thr259, His504, and His499. Among them, Thr259 is one of the residues that composed the gate to the cavity $II_a$, the other two residues are the ligands of the Fe centre. The similarity of the docked position of linoleic acid and the complex **1** indicates that the complex **1** entered the cavity $II_a$ through the gate like linoleic acid. Thus the binding of the complex **1** to LOX-1 is able to block the access of the linoleic acid to the active site, which is consistent with the competitive inhibitory activity of the complex **1** observed in the experiment. Interestingly, when mef was docked with LOX-1, the best docking result is that mef is located inside the cavity $II_a$ (blue molecule in Fig. 5b), but is different from the linoleic acid, and overlapped with one mef ligand of the complex **1** (Fig. 5c). Therefore, the inhibition of mef to LOX-1 is competitive but the inhibitory activity is lower

Table 3 Kinetic parameters of LOX-1 oxidizing linoleic acid in the absence and presence of the complexes **1–3** and Mef

| | $V_{max}$ (M s$^{-1}$) | $K_m$ (M) | $K_{cat}$ (s$^{-1}$) | $K_{cat}/K_m$ (M$^{-1}$ s$^{-1}$) | $K_i$ (M) |
|---|---|---|---|---|---|
| — | $2.35 \times 10^{-7}$ | $1.67 \times 10^{-5}$ | $2.35 \times 10^{2}$ | $1.40 \times 10^{7}$ | 0 |
| **1** | $2.35 \times 10^{-7}$ | $3.72 \times 10^{-5}$ | $2.35 \times 10^{2}$ | $6.41 \times 10^{6}$ | $1.08 \times 10^{-3}$ |
| **2** | $1.23 \times 10^{-7}$ | $1.67 \times 10^{-5}$ | $1.23 \times 10^{2}$ | $7.36 \times 10^{6}$ | $7.52 \times 10^{-4}$ |
| **3** | $1.07 \times 10^{-7}$ | $1.67 \times 10^{-5}$ | $1.07 \times 10^{2}$ | $6.41 \times 10^{6}$ | $3.01 \times 10^{-4}$ |
| mef | $2.35 \times 10^{-7}$ | $2.61 \times 10^{-5}$ | $2.35 \times 10^{2}$ | $9.00 \times 10^{6}$ | $2.71 \times 10^{-4}$ |

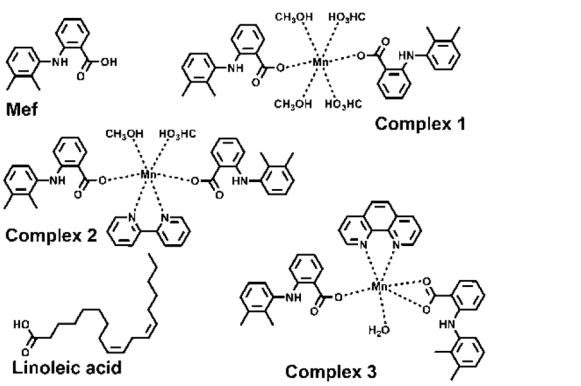


Fig. 4 Chemical structures of three Mn-mef complexes, the ligand mef, and the substrate linoleic acid of LOX-1 used in the docking.

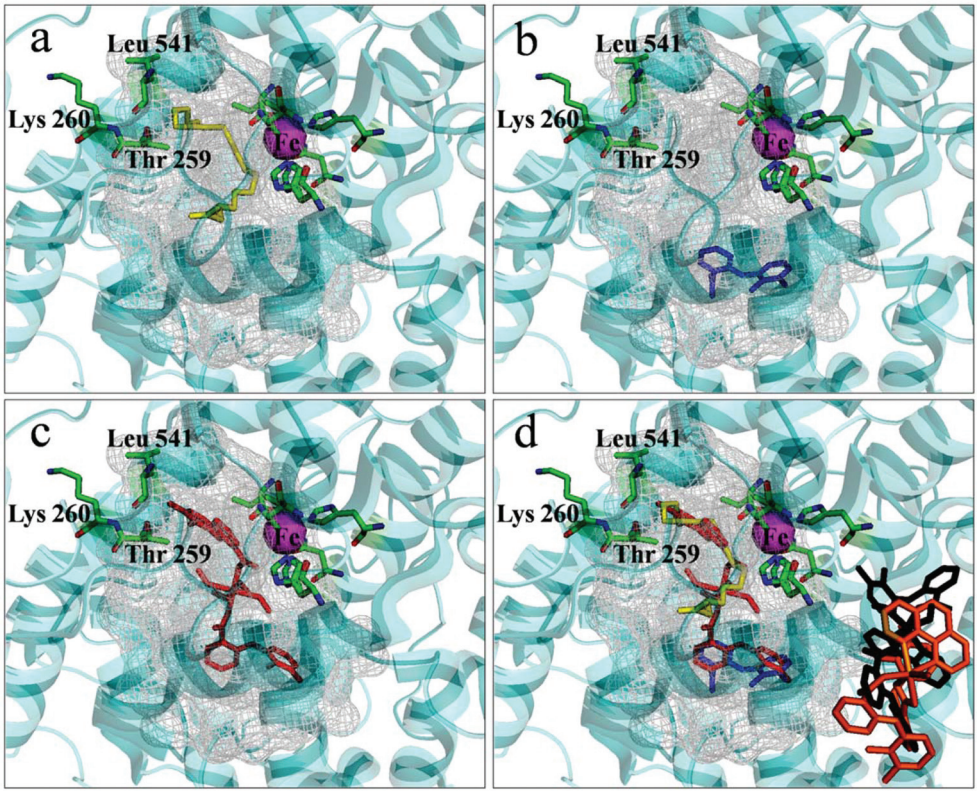


**Fig. 5** The binding modes of linoleic acid, mef, the complexes **1**–**3**, at the cavity $II_a$ (gray net region) of LOX-1. Three residues Thr259, Lys260 and Leu541 that gate the entrance of the cavity $II_a$ are displayed. The active site of LOX-1, and the Fe atom along with its coordination ligands (His 499/504/690, Ile839, and Asn694) are also displayed. (a) Linoleic acid (yellow), (b) mef (blue), (c) complex **1** (red), and (d) overlay of (a), (b), and (c); and the complexes **2** (black) and **3** (orange) that were docked at the outside of the cavity $II_a$.

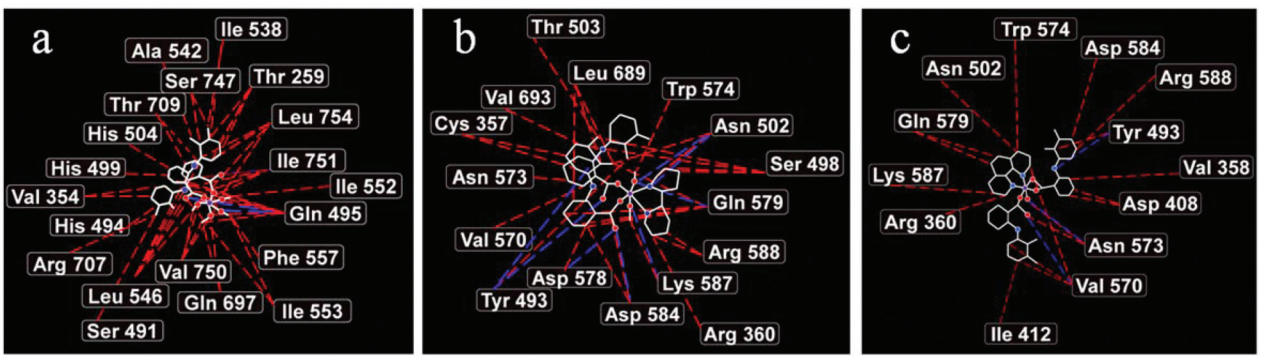


**Fig. 6** Ligand maps of the three complexes binding to the LOX-1 (for clarity, hydrogen bonds with water were excluded, blue dotted lines indicate hydrogen bonds; red dotted lines indicate steric interactions). (a) Complex **1**; (b) complex **2**; and (c) complex **3**.

than that of the complex **1**, which is consistent with the experimental result (Table 3).

In contrast, the complexes **2** and **3** cannot be docked inside the cavity $II_a$ as the complex **1** does. Instead, they can be best docked at a position ~3 Å away from the cavity $II_a$ (Fig. 5d, black and orange molecules outside the cavity $II_a$). The complex **2** interacts with LOX-1 mainly through hydrogen bonds with Tyr493, Asp578, Asp584, Lys587, Gln579, and Asn502 residues (Fig. 6b), and the complex **3** is mainly stabilized by three hydrogen bonds with Tyr493, Val570 and Asn573 (Fig. 6c).

It is possible that other weak interactions between the complex **2** and the residues of LOX-1 also contribute to their interactions. The interaction with these residues may affect the activity of the LOX-1, because they are adjacent to the ligands of the Fe atom. Therefore, the complex **2** exerts its effect on the LOX-1 catalytic activity by affecting the conformation of the active site of LOX-1, which eventually induces the non-competi-

 

tive inhibition of linoleic acid oxidation as observed experimentally. Similarly, the complex **3** also interacts weakly with other residues as shown in Fig. 6c. However, these residues only indirectly interact with the residues that are critical to the activity of LOX-1, therefore the inhibitory activity of the complexes **2** and **3** is much lower than the complex **1**. However, the interactions with the residues need to be further confirmed by the site-directed mutagenesis of LOX-1.

The difference in the binding of the complexes **1–3** to LOX-1 originated from their structural differences. As shown in Fig. 1, two ligands extend from two sides of the octahedral manganese centre in the complex **1**, while the two mef ligands in the complex **2** are oriented in the same direction of the two sides of the Mn-bipy plane, and they are even more expanded in the complex **3**. Thus the bulky complexes **2** and **3** cannot enter the cavity $II_a$ as easily as the complex **1**. Actually, by taking a closer look at the environment of the complex **1** docked inside the cavity $II_a$, one can see that the complex **1** is surrounded closely by the residues Gln495, Leu546, Ile553, and Leu754 (Fig. S2b†); complexes **2** and **3** are definitely too large to fit in this room.

Combining the aforementioned docking and experimental results, we conclude that the inhibitory activity of the Mn-mef complexes **1–3** towards LOX-1 is determined by their binding mode to LOX-1, which is in turn decided by their spatial arrangements. To further confirm this result, we also synthesized Co-mef complexes with similar structures, which have also been reported to exhibit the LOX-1 inhibitory activity.[15] As expected, three Co-mef complexes showed the same inhibition trend as Mn-mef complexes. $Co(mef)_2(CH_3OH)_4$ exhibited a strong competitive inhibition towards LOX-1 as the complex **1**; while $Co(mef)_2(bipy)(CH_3OH)_2$ and $Co(mef)_2(phen)(CH_3OH)_2$ showed weak non-competitive inhibition as the complexes **2** and **3**, respectively (data not shown). These results corroborated unambiguously that the structures of the metal-mef complexes determine their interaction with the enzyme consequently leading to different enzyme inhibitory activities. To this aspect, the role of metal ions in metal-mef is more structural, the unique geometry of the metal-mef complexes orients the ligand to the right binding site of the enzyme. A variety of metal complexes in addition to Mn-mef and Co-mef are necessary to discover the other roles of metal ions; however, different metal complexes may have different structures, which may complicate the question.

### Anti-oxidant activity of the complexes 1–3

As reported for many other metal-NSAID complexes, the anti-oxidant activity of NSAIDs that is closely related to their anti-inflammatory activity usually is improved to a certain extent *via* the coordination to metal ions compared to the parent NSAID ligand.[14] In order to evaluate the anti-oxidant activity of the three Mn-mef compounds, the ability to scavenge free radical DPPH is measured. DPPH with a strong absorption at 517 nm in methanol becomes colourless when accepting an electron,[36] thus the absorption change at 517 nm of DPPH in the presence of the Mn-mef complexes can be used to measure

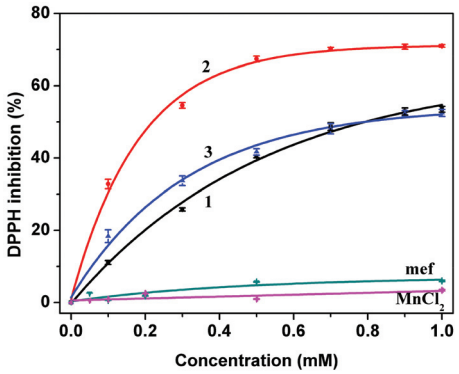


**Fig. 7** Radical scavenging rates *versus* different concentrations of the complexes **1–3**, mef, and $MnCl_2$ in methanol for 30 min. DPPH is 30 μM.

the radical scavenging activity of the complexes. There is a fast decrease phase after adding the complexes **1–3** to DPPH solution in the first ~3 min, and then a gradual change is observed (Fig. S3†). The contribution of manganese ions alone was negligible under this condition. Three complexes showed a similar trend. At different complex concentrations, we found that the free radical scavenging abilities of three complexes are in the order: **2** ≫ **3** and **1**, while the ligand mef and $MnCl_2$ barely exhibit any activity as shown in Fig. 7. These data are comparable to the copper complex; however, it was reported that dinuclear $Cu_2(mef)_4(H_2O)_2$ was much better than the mononuclear complexes.[16] The radical scavenging by the complexes **1–3** was also confirmed by EPR measurements. All three complexes showed a similar behaviour as shown in Fig. S4† using the complex **2** as an example. The EPR signal of DPPH is quenched drastically in the first 3 minutes after the addition of the complex indicating the strong radical scavenging activity of the complex.

The anti-oxidant activity of the complexes was also characterized complementarily by inhibiting the SOD activity. For comparison, the activity of the ligand mef and $MnCl_2$ was measured under the same conditions. Complexes **1–3** exhibit SOD activity inhibition of 65.73%, 82.00%, and 70.14% at a concentration of 0.5 μM, respectively (Fig. S5†), while the ligand mef and $MnCl_2$ exhibit very low activity. Fisher *et al.* reported that Mn-monensin complexes under the same experimental conditions showed the SOD inhibitory activity of 67.5%.[37] The complexes **2** and **3** are again slightly active than the complex **1**, which is consistent with the radical scavenging results.

## Conclusions

Three Mn-mef complexes were synthesized and characterized by UV-visible and IR spectroscopy, elemental analysis, and X-ray crystal diffraction. The pharmaceutical activity of the three complexes was explored in parallel with the parent ligand mef. We found that the Mn-mef complexes exhibited higher LOX-1 inhibitory activity than the ligand mefenamic acid. The inhibi-

tory activity of the complexes is closely related to their spatial arrangements, which decide their interaction modes with the LOX-1. The complex **1** that contains two mef ligands inhibits the enzyme activity competitively, while the bulky and low symmetry complexes **2–3** tend to inhibit the enzyme activity uncompetitively. The computer docking results of the three complexes and the ligand mef with the LOX-1 are highly consistent with the experimental results. The smaller size metal complexes and the ligand itself are likely to bind competitively at the substrate binding site, while the bulky complexes cannot enter the substrate binding site, and thus inhibit the enzyme activity un-competitively *via* binding to the enzyme at different sites. The anti-oxidant activity of the Mn-mef complexes is also improved compared to the parent drug, which is apparently originated from the metal centre. The coordination of mef to manganese ions improves the anti-inflammatory activity of mef by enhancing its LOX-1 inhibitory activity, and/or increasing its anti-oxidant ability *via* the manganese centre. We demonstrated that metal-NSAID complexes are better anti-inflammatory drug candidates than NSAIDs, because they have unique structures that could interact with the target enzymes more specifically. In addition, metal ions introduce extra anti-oxidant activity to metal-NSAID complexes.

## Acknowledgements

This research was carried out with financial support from the National Science foundation of China (no. 21001044 and 31070742), the State Key Laboratory of Bioreactor Engineering (no. 2060204), 111 Project (no. B07023), and the Shanghai Committee of Science and Technology (no. 11DZ2260600).

## References

1 C. P. Duffy, C. J. Elliott, R. A. O'Connor, M. M. Heenan, S. Coyle, I. M. Cleary, K. Kavanagh, S. Verhaegen, C. M. O'Loughlin, R. NicAmhlaoibh and M. Clynes, *Eur. J. Cancer*, 1998, **34**, 1250–1259.
2 F. Catella-Lawson, M. P. Reilly, S. C. Kapoor, A. J. Cucchiara, S. Demarco, B. Tournier, S. N. Vyas and G. A. Fitzgrerald, *N. Engl. J. Med.*, 2001, **345**, 1809–1817.
3 J. R. Vane and Regina M. Botting, *Am. J. Med.*, 1998, **104**, 2S–8S.
4 L. A. G. Rodriguez, *Clin. Exp. Rheumatol.*, 2001, **19**, S41–S44.
5 I. Bjamason, J. Hayllar, A. J. MacPherson and A. S. Ressell, *Gastroenterology*, 1993, **104**, 1832–1847.
6 P. Amadio, D. M. Cummings and P. Amadio, *Postgrad. Med.*, 1993, **93**, 73–97.
7 N. Ouyang, P. Ji and J. L. Williams, *Int. J. Oncol.*, 2012, **42**, 643–650.
8 M. Elkady, R. Nieß, A. M. Schaible, J. Bauer, S. Luderer, G. Ambrosi, O. Werz and S. A. Laufer, *J. Med. Chem.*, 2012, **55**, 8958–8962.
9 J. E. Weder, C. T. Dillon, T. W. Hambley, B. J. Kennedy, P. A. Lay, J. R. Biffin, H. L. Regtop and N. M. Davies, *Coord. Chem. Rev.*, 2002, **232**, 95–126.
10 C. T. Dillon, T. W. Hambley, B. J. Kennedy, P. A. Lay, Q. D. Zhou, N. M. Davies, J. R. Biffin and H. L. Regtop, *Chem. Res. Toxicol.*, 2003, **16**, 28–37.
11 M. Konstandinidou, A. Kourounakis, M. Yiangou, L. Hadjipetrou, D. Kovala-Demertzi, S. Hadjikakou and M. Demertzis, *J. Inorg. Biochem.*, 1998, **70**, 63–69.
12 A. S. Fernandes, J. Gaspar, M. F. Cabral, C. Caneriras, R. Guedes, J. Rueff, M. Castro, J. Costa and N. G. Oliverira, *J. Inorg. Biochem.*, 2007, **101**, 849–858.
13 C. V. Winder, J. Wax, L. Scotti, R. A. Scherrer, E. M. Jones and F. W. Short, *J. Pharmacol. Exp. Ther.*, 1962, **138**, 405–413.
14 D. Kovala-Demertzi, D. Hadjipavlou-Litina, M. Staninska, A. Primikiri, C. Kotoglou and M. A. Demertzis, *J. Enzyme Inhib. Med. Chem.*, 2009, **24**, 742–752.
15 F. Dimiza, A. N. Papadopoulos, V. Tangoulis, V. Psycharis, C. P. Raptopoulou, D. P. Kessissoglou and G. Psomas, *Dalton Trans.*, 2010, **39**, 4517–4528.
16 F. Dimiza, S. Fountoulaki, N. P. Athanasios, C. A. Kontogiorgis, V. Tangoulis, C. P. Raptopoulou, V. Psycharis, A. Terzis, D. P. Kessissoglou and G. Psomas, *Dalton Trans.*, 2011, **40**, 8555–8568.
17 V. Dokorou, A. Primikiri and D. Kovala-Demertzi, *J. Inorg. Biochem.*, 2011, **105**, 195–201.
18 B. P. Skowronska, R. Kaczorowska and T. Skowronski, *Environ. Pollut.*, 1997, **97**, 65–69.
19 D. Hamai and S. C. Bondy, *Neurochem. Int.*, 2004, **44**, 223–229.
20 E. J. Underwood, *Trace Element in Human Health and Animal Nutrition*, Academic press, New York, 4th edn, 1977.
21 B. K. Wagnont and S. C. Jackels, *Inorg. Chem.*, 1988, **28**, 1923–1927.
22 B. Axelrod, T. M. Cheesbrough and S. Laakso, *Methods Enzymol.*, 1981, **71**, 441–451.
23 W. Minor, J. Steczko, B. Steczko, Z. Otwinowski, J. T. Bolin, R. Walter and B. Axelrod, *Biochemistry*, 1996, **35**, 10687–10701.
24 R. Thomsen and M. H. Christensen, *J. Med. Chem.*, 2006, **49**, 3315–3321.
25 E. Vrontaki, G. Leonis, M. G. Papadopoulos, M. Simcic, S. G. Grdadolnik, A. Afantitis, G. Melagraki, S. K. Hadjikakou and T. Mavromoustakos, *J. Chem. Inf. Model.*, 2012, **52**, 3293–3301.
26 M. Saldias, V. Paredes-Garcia, A. Vega, W. Cañon Mancisidor, F. E. Le, D. V. Yazigi and E. Spodine, *Polyhedron*, 2012, **41**, 120–126.
27 X. J. Jiang, H. Liu, B. Zheng and J. Y. Zhang, *Dalton Trans.*, 2009, 8714–8723.
28 R. G. Kurumbail, A. M. Stevens, J. K. Gierse, J. J. McDonald, R. A. Stegeman, J. Y. Pak, D. Gildehaus, J. M. Iyashir, T. D. Penning, K. Seibert, P. C. Isakson and W. C. Stallings, *Nature*, 1996, **384**, 644–648.
29 S. Fiorucci, R. Meli, M. Bucci and G. Cirino, *Biochem. Pharmacol.*, 2001, **62**, 1433–1438.
30 V. C. Ruddat, S. Whitman, T. R. Holman and C. F. Bernasconi, *Biochemistry*, 2003, **42**, 4172–4178.

 

31 H. W. Gardner, *Biochim. Biophys. Acta*, 1989, **1001**, 274–281.
32 J. M. LaLonde, D. A. Bernlohr and L. J. Banaszak, *Biochemistry*, 1994, **33**, 4885–4895.
33 A. C. M. Young, G. Scapin, A. Kromminga, S. B. Patel, J. H. Veerkamp and J. C. Sacchettini, *Structure*, 1994, **2**, 523–534.
34 J. C. Boyington, B. J. Gaffney and L. M. Amzel, *Science*, 1993, **260**, 1482–1486.
35 M. L. Connolly, *Science*, 1983, **221**, 709–713.
36 M. S. Blois, *Nature*, 1958, **181**, 1199–1200.
37 A. E. O. Fisher, G. Lau and D. P. Naughton, *Biochem. Biophys. Res. Commun.*, 2005, **329**, 930–933.